Palaeogeography, Palaeoclimatology, Palaeoecology 641 (2024) 112129

Contents lists available at ScienceDirect

Palaeogeography, Palaeoclimatology, Palaeoecology

journal homepage: www.elsevier.com/locate/palaeo

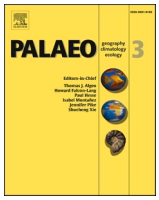

The impact of frequent wildfires during the Permian–Triassic transition: Floral change and terrestrial crisis in southwestern China

Fanghui Hua [a], Longyi Shao [a,**], Xuetian Wang [a], Timothy P. Jones [b], Tianchang Zhang [a], David P.G. Bond [c], Zhiming Yan [d], Jason Hilton [e,f,*]

[a] State Key Laboratory for Fine Exploration and Intelligent Development of Coal Resources and College of Geoscience and Surveying Engineering, China University of Mining and Technology (Beijing), Beijing 100083, China
[b] School of Earth and Environmental Sciences, Cardiff University, Cardiff CF10 3YE, Wales, UK
[c] School of Environmental Sciences, University of Hull, HU6 7RX, UK
[d] School of Civil Engineering and Transportation, Weifang University, Weifang 261061, Shandong Province, China
[e] School of Geography, Earth and Environmental Sciences, University of Birmingham, Edgbaston B15 2TT, UK
[f] Birmingham Institute of Forest Research, University of Birmingham, Edgbaston B15 2TT, UK

ARTICLE INFO

Keywords:
Permian–Triassic terrestrial crisis
Wildfire
Wildfire type
Southwestern China
Floral change

ABSTRACT

Wildfires are considered to have played an important role in the land plants crisis during the Permian–Triassic (P–T) transition. However, the nature and impact of wildfires in the P–T terrestrial crisis remains unclear. Organic petrology data from a terrestrial sequence from southwestern China show that the inertinite content ranges from 21.3% to 80.9% (mean 44.5%), suggesting that wildfires were a frequent phenomenon in low-latitude tropical rainforests during the P–T transition. Abundant inertinite and Hg/TOC peaks in earliest Triassic strata support the co-existence of wildfires and volcanism at that time. Volcanic emissions were potentially lethal for plants and adjacent arc volcanism represents a possible source of ignition. Inertinite reflectance values are used to estimate wildfire combustion temperatures, which themselves are a function of wildfire type. Inertinite with reflectances higher than 4.5% have concentrations between 47% and 65% in the P–T transitional strata. Crown fires with high combustion temperatures were prevalent in wetland settings in the latest Permian. However, surface fires with lower combustion temperatures became dominant during the major terrestrial extinction phase as a result of the sparse, scrubby vegetation that dominated at that time. The subsequent spread of gymnosperms in the earliest Triassic resulted in the re-establishment of high-temperature crown fires. Wildfires associated with the onset of volcanism in the late Permian likely contributed to ecological disturbance in terrestrial settings, which occurred notably earlier than that seen in marine environments. Thus, enhanced wildfire activity destabilised wetlands and increased ecological stress in the late Permian. Wildfire activity on land potentially had devastating consequences for late Permian marine environments via a complex cascade of terrestrial denudation, runoff, and nutrient flux.

Editor: S Shen

1. Introduction

Wildfires are common and widespread in the modern world (Jolly et al., 2015; Kelly et al., 2020), and the fossil record of wildfires extends back in time at least as far as the Silurian (Bowman et al., 2009; Glasspool et al., 2015). Wildfires impose ecological stress on a variety of terrestrial systems (Kelly et al., 2020; Mays and McLoughlin, 2022). Extensive wildfires can potentially threaten the stability of forests and disrupt hydrological cycles, resulting in an abrupt decline in biodiversity (Shao et al., 2012; Vajda et al., 2020). In recent years, an increased occurrence and severity of wildfires resulted in habitat loss and the deaths of large numbers of animals in southeastern Australia (2019–2020), western United States (2020), far east Russia (2021), and western Europe (2022), demonstrating the destructive power of wildfires (https://firms.modaps.eosdis.nasa.gov/map/). Elevated air temperatures and reduced summer precipitation are generally considered to

* Corresponding author at: School of Geography, Earth and Environmental Sciences, University of Birmingham, Edgbaston B15 2TT, UK.
** Corresponding author.
E-mail addresses: ShaoL@cumtb.edu.cn (L. Shao), j.m.hilton@bham.ac.uk (J. Hilton).

https://doi.org/10.1016/j.palaeo.2024.112129
Received 25 November 2023; Received in revised form 2 March 2024; Accepted 4 March 2024
Available online 6 March 2024

be the main causes of increased fire-prone conditions (He and Lamont, 2018) and it is notable that increased palaeo-wildfire activity correlates with periods of global warming hyperthermal events during several past extinction crises (Vajda et al., 2001; Lindström, 2021; Baker, 2022).

At the end of the Paleozoic, Earth experienced its most severe mass extinction, which devastated global faunas and floras (Benton and Newell, 2014; Dal Corso et al., 2022). Volcanically-driven environmental change is generally considered the key driver of the Permian–-Triassic mass extinction (PTME) (Kamo et al., 2003; Burgess et al., 2017; Zhang et al., 2021). A globally-widespread, major negative carbon isotope excursion and various extinction mechanisms have been attributed to the release of volcanogenic and thermogenic gases associated with the Siberian Traps large igneous province (STLIP) (Chen and Benton, 2012; Benton and Newell, 2014). Low latitude sea surface temperatures warmed as much as 10 °C between the latest Permian and Early Triassic (Wang et al., 2020a) with devastating consequences for marine life (Sun et al., 2012; Song et al., 2013; Stanley, 2016). Elevated levels of inertinite/charcoal (Cai et al., 2021a; Lu et al., 2022; Song et al., 2022) and polycyclic aromatic hydrocarbons [PAHs] (Jiao et al., 2023) in strata from this interval suggests that this atmospheric hyperthermal event promoted forest fires. Evidence for elevated wildfire activity has been reported across the P–T boundary in sections in numerous regions, with enhanced wildfires probably a global phenomenon during the PTME interval (Shen et al., 2011; Vajda et al., 2020; Cai et al., 2021a; Lu et al., 2022; Mays and McLoughlin, 2022).

From a terrestrial crisis process perspective, the cause-and-effect roles of wildfires are still unclear. Some studies suggest that intense wildfires significantly impacted P–T terrestrial ecosystems (Yan et al., 2019; Vajda et al., 2020). An increase in wildfire activity has been linked to the earlier onset of the crisis in terrestrial settings when compared to marine environments in the latest Permian (Lu et al., 2022). In contrast, others point out that fire was a common feature of forest ecosystems and played an ecological role in plant evolution and in shaping functional types (He and Lamont, 2018). High inertinite/charcoal abundances are found in strata below and above the level of the terrestrial PTME (Chu et al., 2020; Cai et al., 2021b; Zhou et al., 2021), suggesting that recurrent wildfires were a feature of a volcanogenic extinction scenario rather than the ultimate cause of the terrestrial PTME. Deforestation by frequent wildfires is plausible, but wildfires probably played a variety of roles – not all destructive – in forest ecosystems before, during, and after the terrestrial PTME.

Southwestern China was a location of stable peatland ecosystems in the late Permian, and this area became the ultimate refuge of the Paleozoic fern-dominated Cathaysian (*Gigantopteris*) Flora (Broutin et al., 2020; Feng et al., 2020). Tropical low palaeolatitude rainforests provided an important habitat for terrestrial animals, and these forests were the main contributor to the widespread accumulations of late Permian coals in southern China (Peng et al., 2006; Yu et al., 2015). The terrestrial PTME resulted in the replacement of stable pteridophyte-dominated floras with rapidly growing communities dominated by lycopods (Yu et al., 2015; Feng et al., 2020; Xu et al., 2022; Dal Corso et al., 2022; Shao et al., 2023). There is increasing evidence that wildfires were a common feature of the vegetation shift interval in this region (Chu et al., 2020; Cai et al., 2021b; Jiao et al., 2023) while strata in the area reveal anomalously high mercury (Hg) concentrations, possibly of volcanic origin (Shen et al., 2019a; Zhang et al., 2021; Chen et al., 2023). Charcoal, the product of incomplete combustion of plant material during wildfire, provides valuable information on the occurrence of wildfires in the geological past (e.g., Batten, 1996; Lu et al., 2020; Xu et al., 2022). Inertinite is recognised as synonymous with charcoal and is now widely used as a proxy for wildfire activity in the geological record (Scott and Glasspool, 2007). High contents of inertinite are observed in P–T strata in southwestern China. This region provides an excellent opportunity to study of the relationship between volcanism, ancient wildfires and the evolution of terrestrial forests during the terrestrial PTME. This study is based on a continuously cored borehole record of late Permian to Early Triassic strata from a low palaeolatitude setting near Xuanwei city, eastern Yunnan Province. We integrate geochemical data with analysis of organic macerals and palaeontology to explore the role of wildfires in a volcanically-driven terrestrial mass extinction scenario.

2. Geological setting and background

Southwestern China is on the western margin of the South China Block (Zhang et al., 2013) that at the end of the Permian was located near the equator (Huang et al., 2018). Tectonically, the region was within the influence range of the Tethyan Realm (Riel et al., 2018) (Fig. 1a). During the middle and late Permian, the region was affected by the expansion of the Palaeo-Tethys Ocean (Zhang et al., 2013) and the emplacement of the Emeishan large igneous province (Ali et al., 2005). The continuously uplifting Khangdian Oldland was the main sediment source in southwestern China (Wang et al., 2020b). Constrained by the Khangdian Oldland, and with transgressions and regressions from the east and southeast, the region experienced a succession of terrestrial, transitional and marine depositional conditions during the late Permian to Early Triassic (Shao et al., 2020) (Fig. 1b).

The core samples used in this study were collected from borehole H401, drilled in the Hanjiagou area of Xuanwei city, eastern Yunnan Province (26° 25′ 32.846″ N, 104° 15′ 10.565″ E; Fig. 1b, c). The region had a humid and warm climate, and temperatures increased rapidly during the latest Permian (Wang et al., 2020a). Macro- and microfloras indicate that a humid and warm climate regime prevailed in the earliest Triassic (Yu et al., 2015), but the longer-term climatic trend was towards more arid conditions. Atmospheric oxygen concentrations were maintained at high levels during the late Permian to Early Triassic (Fig. 2) (Krause et al., 2018), with important implications for the increased occurrence and severity of wildfires.

The late Permian to Early Triassic terrestrial succession in this region is comprised of the Xuanwei, Kayitou and Dongchuan formations in ascending stratigraphic order. The Xuanwei Formation is composed of mudstone (the clay-sized component is >50% of the total), siltstone (the silt-sized component is >50%), sandstone, and coal seams, and is rich in ferns from the Cathaysian palaeo-flora that includes *Gigantopteris*, *Lobatannularia*, and *Pecopteris* (Yu et al., 2015). The uppermost coal (the C_1 coal at the top of the Xuanwei Formation) records the final accumulation of peat during the PTME event, and zircon U—Pb dating places the P–T boundary within this coal (Wang et al., 2018) (Fig. 2), an age assignment further confirmed by chemical abrasion-isotope dilution-thermal ionization mass spectrometry analysis (CA-ID-TIMS) (Wu, 2020; see also Wu et al., 2024). However, due to the sedimentary variability of terrestrial strata and the discontinuous distribution of the C_1 coal across the region, there remain uncertainties in correlating numerous stratigraphic sections in the region with the marine Global Boundary Stratotype Section and Point (GSSP) at Meishan (Zhang et al., 2016; Shen et al., 2019b; Zhang et al., 2021).

Above the Xuanwei Formation, the Kayitou Formation consists of greenish-grey mudstone and siltstone, and coal is absent (Fig. 2). The abrupt replacement of the diverse *Gigantopteris* flora community with one dominated by *Tomiostrobus* (*Annalepis*) and *Peltaspermum* at the formational contact is interpreted as the result of widespread and catastrophic disruption of terrestrial ecosystems (Yu et al., 2015; Feng et al., 2020; Xu et al., 2022). The well-known negative carbon isotope excursion and peaks in Hg/TOC are generally recorded in this interval, suggesting that terrestrial ecological disturbances were volcanogenic in origin (Shen et al., 2019a; Chu et al., 2020; Wang et al., 2021; Zhang et al., 2021). In borehole H401, two negative $\delta^{13}C_{org}$ excursions and three Hg/TOC anomalies have been reported from the Kayitou Formation (Fig. 3) (Hua et al., 2023). In addition, the calculated denudation rate for basaltic landscapes (a proxy for volumes of exposed soil resulting from deforestation) experienced two phases of accelerated erosion during a ~ 1 Ma period (Fig. 3) (Hua et al., 2023). The presence

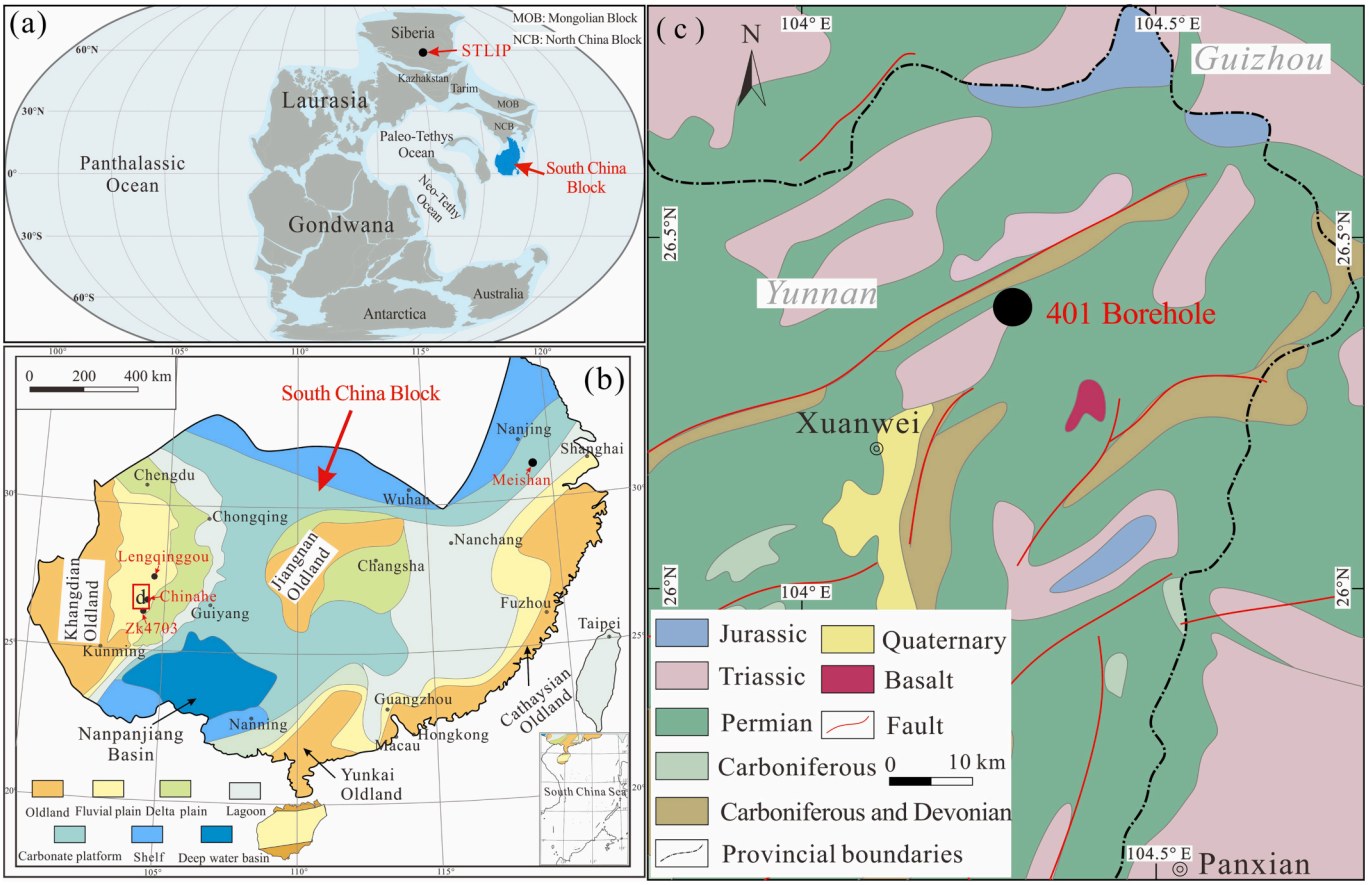

Fig. 1. Location of the South China Plate and palaeogeography of the late Permian. a. Palaeogeographic configuration and the position of the South China Plate (Huang et al., 2018), b. Palaeogeography of South China in the Changhsingian (Shao et al., 2020) and location of the P–T section; c. Map of eastern Yunnan showing the distribution of strata and location of the sampled borehole.

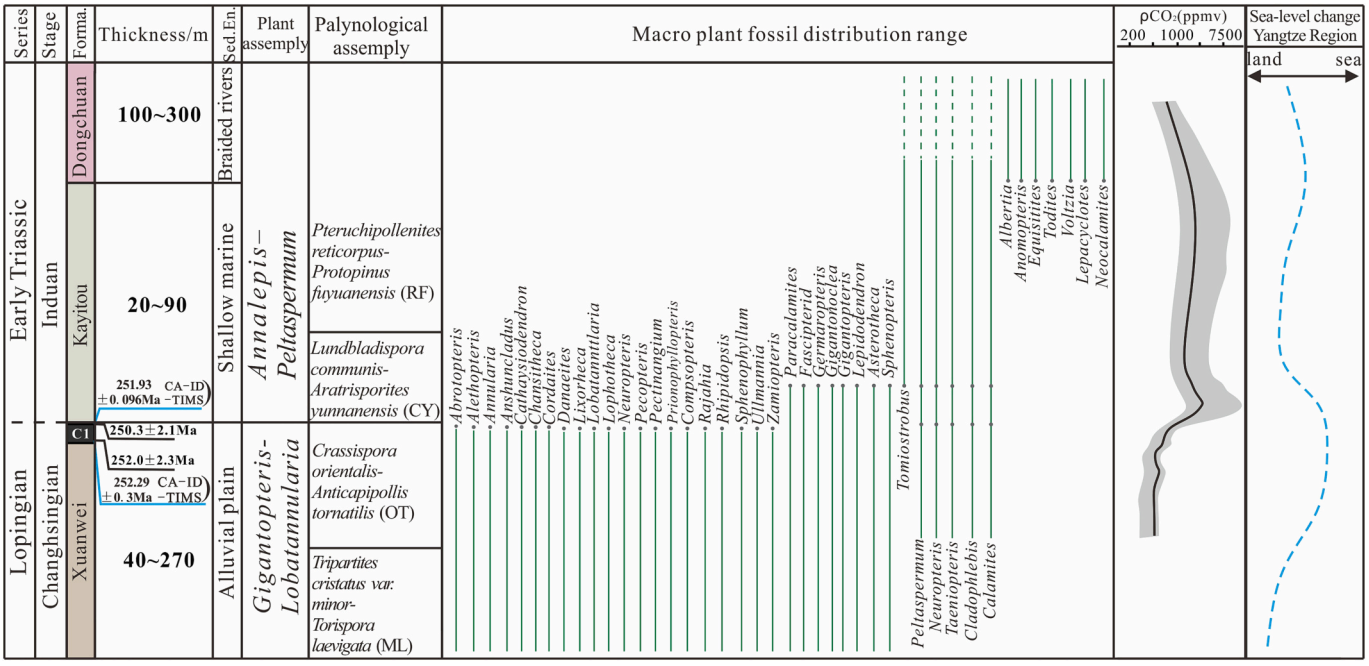

Fig. 2. Stratigraphic framework for the P–T boundary strata from Xuanwei City, Yunnan Province. Age data from Wang et al. (2018) and Wu et al. (2024), sedimentary environments from Shao et al. (2013) and Bercovici et al. (2015), plant assemblages from Yu et al. (2015) and Shao et al. (2023), vertical distribution of plant fossils from Zhang et al. (2016) and Chu et al. (2016), atmospheric O_2 from Krause et al. (2018), Shao et al. (2012) and Glasspool and Scott (2010), sea-level change from Yin et al. (1994) and Shao et al. (2013).

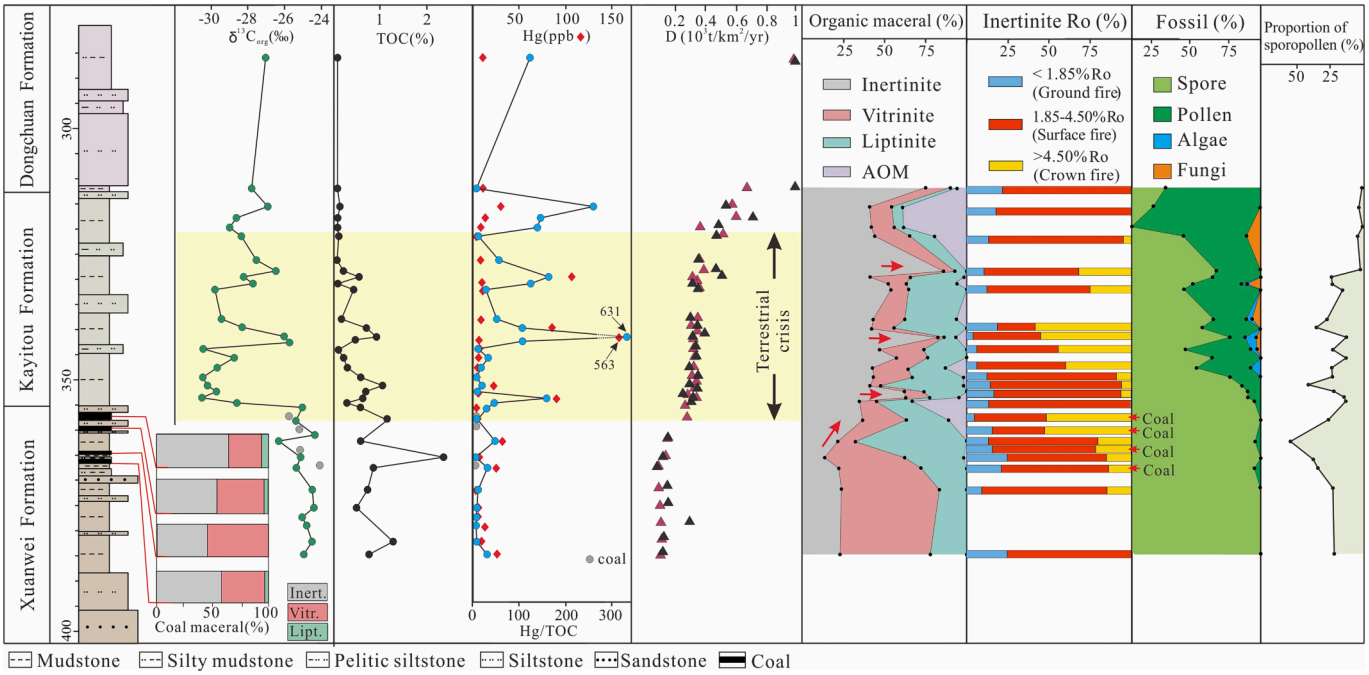

Fig. 3. Stratigraphy and variations of coal macerals, kerogen macerals, inertinite reflectance, and fossil components in the H401 core. Organic carbon isotopes ($\delta^{13}C_{org}$), total organic carbon (TOC), Hg/TOC, and denudation rate (D) in the core are from Hua et al. (2023).

of conchostracans and bivalves in the middle and upper parts of the Kayitou Formation indicates that the environment of deposition had shifted from terrestrial to coastal or shallow marine (Chu et al., 2016).

The overlying Dongchuan Formation is dominated by red-coloured mudstone, siltstone, and sandstone that were deposited in a braided fluvial setting (Bercovici et al., 2015), and the prevailing arid climate resulted in a lack of organic matter and a near total lack of fossils at this level (Fig. 2).

3. Material and methods

Systematic sampling was conducted from strata 50 m above and below the contact between the Xuanwei Formation and overlying Kayitou Formation in the H401 borehole core (Fig. 3). A total of 39 samples were collected, including mudstones (siliciclastic rocks with >50% clay-sized component) and coals from the Xuanwei Formation, and mudstones from the Kayitou and Dongchuan formations.

The organic maceral identification of 35 mudstone samples was conducted at the State Key Laboratory Coal Resources and Safe Mining (Beijing), and this same material was also used for spore-pollen analysis. Approximately 50 g per sample were crushed to around 0.5 mm, and subsequently treated with hydrochloric (HCl) and hydrofluoric (HF) acids to remove carbonates and silicates. The residues were centrifuged and sieved with a 5 μm nylon mesh. The remaining organic residue was divided into two parts. One part was mounted in epoxy resin on microscopy slides and analysed using transmitted light microscopy (Olympus BX 41). The organic macerals were classified according to China's national standard (SY/T5125–2014), with no less than 300 effective points per sample. Another fraction of each sample was used for reflected light microscopy. The reflectance of inertinite was measured under oil immersion at 500× magnification using a Zeiss MPV-III reflected light microscope with a microphotometer following standard procedures. At least 100 valid points of discrete inertinite fragments were measured from each sample. Three mudstone samples were found to have no organic components.

Coal samples were subjected to maceral identification and reflectance measurements. The coal samples were crushed and sieved to between 63 μm and 1 mm to make polished blocks, and microscopic observations were performed under oil immersion at 500× magnification using a Zeiss MPV-III reflected light microscope. At least 300 valid points were counted for each coal sample, following the maceral classification scheme proposed by the International Committee for Coal and Organic Petrology (ICCP System, 2001). The reflectance measurement techniques for inertinite in coal were the same as those used for the organic matter extracted from mudstone. Since the organic microfractions are classified differently in mudstone and coal, we present the data in two tables (Tables S1 and S2). However, the inertinite in both types of rock are used to indicate wildfire events (Lu et al., 2022), so we compare them in a single figure. All polished blocks are housed at the State Key Laboratory of Coal Resources and Safe Mining (Beijing). The same samples were analysed for carbon isotopes, TOC, and Hg concentrations by Hua et al. (2023) and these data are included here to facilitate integration of the wildfire record with that of volcanism.

4. Results

4.1. Organic macerals in coal

One sample was taken from each of the four thin coal seams in the uppermost part of the Xuanwei Formation (Fig. 3). On a mineral-matter-free basis, these coal samples contain abundant inertinite, less abundant vitrinite, and a minor component of liptinite. Vitrinite has relative contents ranging from 29.7% to 42.1% (mean 36.4%), and the vitrinite macerals are characterised by grey, non-structural or structural macerals under reflected light, including telovitrinite, detrovitrinite and gelovitrinite (Fig. 4a and b). Liptinite has relative contents ranging from 0% to 6% (mean 3.21%) and the liptinite macerals are characterised by dark grey to black macerals under reflected light, including sporinite, resinite, and liptodetrinite (Fig. 4a, b).

Inertinite is a major component of each coal sample with relative contents ranging from 45.0% to 64.3% (mean 55.3%). Within the inertinites, fusinite and semifusinite are the most abundant fractions (mean 27.1% and 20.4%, respectively), followed by inertodetrinite (mean 6.1%) while other inertinites, including macrinite, and funginite, account for <5% (mean of these = 1.8%) (Fig. 4c, d, e and f). Under reflected light fusinite and semifusinite are highly reflective and show

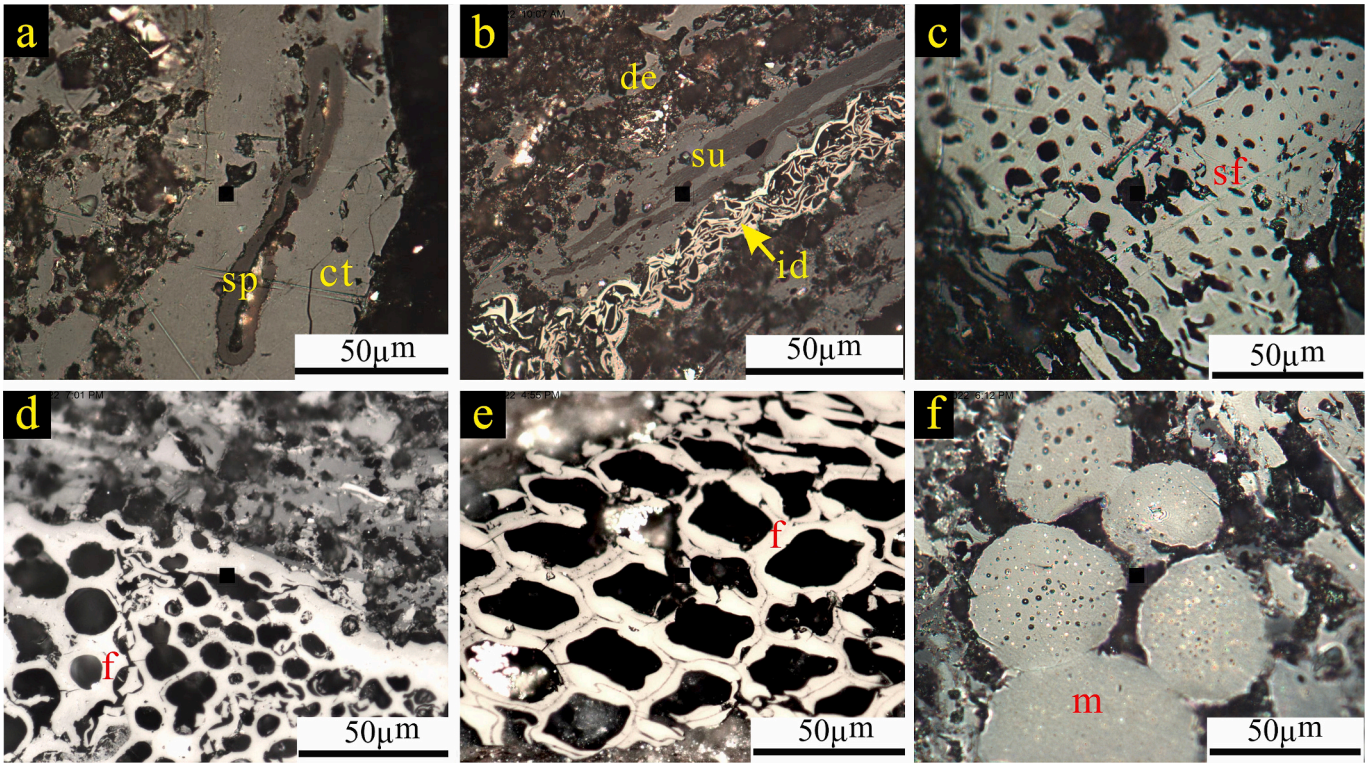

Fig. 4. Photomicrographs showing microstructure characteristics (reflected light). a showing characteristics of vitrinite and liptinite from sample X-5 (ct-collotelinite and sp-sporinite); b showing characteristics of vitrinite, inertinite and liptinite from X-8 (de-detrovitrinite, su- suberinite, id- inertodetrinite); c showing characteristics of semifusinite from sample X-3 (sf- semifusinite); d and e showing characteristics of fusinite from sample X-2 and X-1 (f- fusinite); f showing characteristics of macrinite from X-8 (m- macrinite).

well-preserved cellular structures (Fig. 4c, d and e). The inertinite content shows an irregular but generally increasing trend upwards in the succession, with a sharp increase at the top of the Xuanwei Formation where contents reach 64%. The inertinite content in coals near the top of the Xuanwei Formation increases significantly with values similar to the inertinite contents in the C_1 coal reported by Yan et al. (2019).

4.2. Organic macerals in mudstone

Organic macerals in the mudstone samples are dominated by inertinite, followed by vitrinite and liptinite, with a little amorphous organic matter (Fig. 3 and Table S2). Relative contents of vitrinite vary from 2.0% to 55.9% (mean 20.6%), and the vitrinite macerals are mainly black or brown particles showing brown margins under transmitted light (Fig. 5b). The relative contents of liptinite vary from 3.1% to 69.1% (mean 27.4%) and the liptinite macerals are mainly cuticle fragments (Fig. 5a), spores and pollen (Fig. 5f, g and h), fungi and algae (Fig. 5d and e). Inertinite content ranges between 21.3% and 80.9% (mean 44.5%) and under transmitted light, the inertinite macerals are entirely opaque and fragmental, with most being long and thin with sharp edges (Fig. 5c). The amorphous organic matter is characterised by brown floc (Fig. 5i). The relative contents of the amorphous organic matter are low, ranging from 0% to 43.1% (mean 6.8%). Taken in ascending stratigraphic order the relative contents of fusinite in mudstone increases significantly near the top of the Xuanwei Formation and three obvious inertinite peaks with values of 71.1%, 80.9% and 87.8% occur in the Kayitou Formation (Fig. 3). The inertinite content in mudstones at the top of the Xuanwei Formation and in the overlying Kayitou Formation are significantly higher than those in the rest of the Xuanwei Formation (Fig. 3). Previous research indicates that during deposition of the Kayitou Formation, the sedimentary environment shifted from terrestrial to coastal or shallow marine, and therefore the organic components of the mudstone were not influenced by co-sedimentary oxidation. The organic fragments in these mudstones contain a variety of plant materials (wood, cuticle and sporopollen) and sizes (500 μm–1 mm), implying minimal transport (Scott, 2010). Therefore, the characteristics of the inertinite likely reflect local wildfire events.

Spores, pollen, algae, and fungi were observed in the studied samples, but their genera and species were not differentiated. Instead, the relative contents of spores and pollen were used to infer changes in the plant communities. Spores are dominant in the Xuanwei Formation, which is almost free of pollen (Fig. 3), while in the Kayitou Formation, the proportion of pollen gradually increases before becoming dominant in the middle part of the Formation (Fig. 3). In the upper part of the Kayitou Formation, pollen is almost exclusively observed in the near total absence of spores, but in exceedingly small quantities (Fig. 3). These results suggest that the fern-dominated *Gigantopteris* floral community that thrived during deposition of the Xuanwei Formation was gradually replaced by a gymnosperm-dominated community.

4.3. Inertinite reflectance and likely wildfire types

Since inertinite (charcoal) reflectance is influenced by combustion temperature, the burning temperature of wildfires can be inferred from inertinite reflectance values (Jones, 1997; Scott and Glasspool, 2005; Belcher and Hudspith, 2016). Although experimental oven charring research has shown that the relationship between inertinite reflectance and burning temperature is not linear, the burning temperature can be estimated from inertinite reflectance by the linear regression equation: $T = 184.10 + 117.76 \times R_o$ (coefficient of determination $r^2 = 0.91$), where T represents the burning temperature (°C) and R_o is the mean random inertinite reflectance as measured under oil (%) (Jones, 1997). This linear regression equation was later updated based on data from Scott and Glasspool (2005) by Yan et al. (2019) as follows:

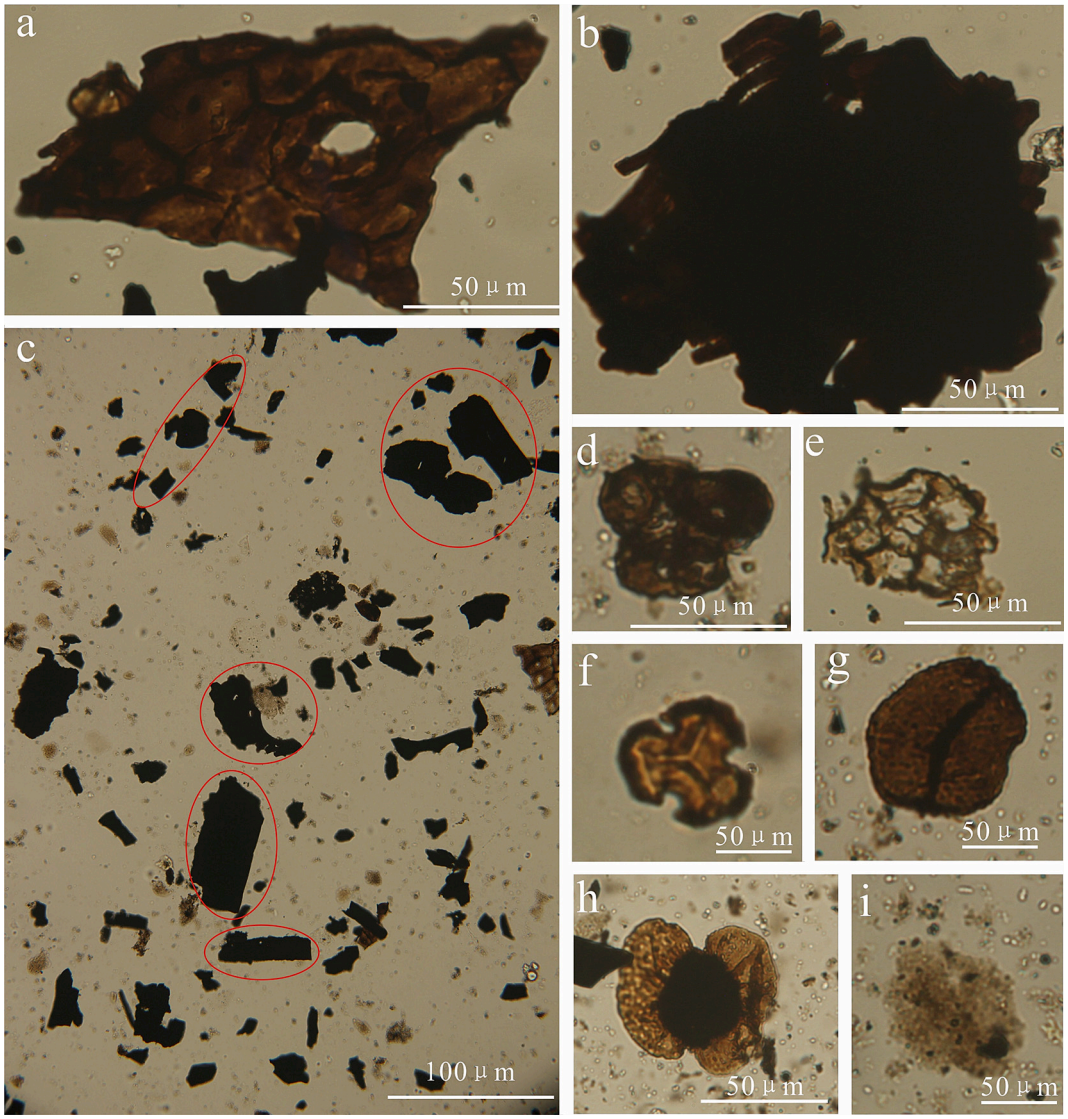

Fig. 5. Photomicrographs showing microstructure characteristics of organic residue (transmitted light). a cuticle fragment showing stoma from sample K-34; b vitrinite fragment from sample X-9; c inertinite in the red circle from sample K-33; d fungi from sample K-29; e algal thalli from sample K-41; f and g spore from sample X-7; h pollen from sample K-36; i amorphous organic matter from sample K-41. (For interpretation of the references to colour in this figure legend, the reader is referred to the web version of this article.)

$$T = 224.53 + (94.975 \times R_o) \quad (1)$$

$r^2 = 0.9606$

It is important to note that there is one piece of empirical measured data from the fossil material, the R_o, which is influenced by a range of factors of which temperature is considered the most important (Jones and Chaloner, 1991). However, the duration of the burns, meteorology (windiness), and the nature of the vegetation are also key variables. Depending on the derived burning temperatures and identification of the combustible materials, three basic types of wildfires can be inferred, namely crown, surface, and ground fires (Scott, 1989). Crown fires have high burning temperatures, ranging from 650 °C to 800 °C; $R_o > 4.5\%$, although modern crown fires have recorded much higher temperatures (Alexander et al., 1998). Experimental work by Jones et al. (1991) showed that combustion above 800 °C resulted in complete combustion and no residual charcoal. Surface fires have moderate burning temperatures (mostly ranging from 400 °C to 650 °C; R_o 1.85–4.5%), while ground fires have low burning temperatures (mostly <400 °C; $R_o <$ 1.85%) (Scott, 1989; Jones et al., 1991; Scott and Glasspool, 2005). Using derived burning temperatures to determine the type of wildfire is speculative because there are phases of combustion in wildfires of any intensity, and there are overlaps of temperature ranges for each of these wildfire types (Scott, 1989). In order to better understand the palaeo-wildfire scenario at the time, the reflectance of no less than 100 inertinite fragments from each sample was counted to better constrain the various burning temperatures of the fire during the wildfire event. It is noted that, with increased organic coalification, the difference in reflectance among different components will decrease, so it is impossible to be certain that the reflectance values are solely a function of combustion temperatures (ICCP System, 2001). However, in this study, the vitrinite reflectance of all samples is <1%, which is of low to medium rank (Table S2) and therefore organic coalification is not expected to have affected the inertinite reflectance. Overall, inertinite with reflectance between 1.85% and 4.5% is most common, followed by inertinite with reflectance >4.5%. Inertinite with reflectance <1.85% is the least abundant component (Table S2). Thus, relative contents of inertinite with reflectance <1.85% vary from 3.4% to 24.6% (mean 15.4%). Relative contents of inertinite with reflectance 1.85% to 4.5% vary from 24.1% to 87.3% (mean 62.4%). Relative contents of inertinite with

reflectance >4.5% vary from 0% to 65.4% (mean 22.2%). Two levels of abundant high reflectance inertinite are seen in the upper part of the Xuanwei Formation and the lower part of the Kayitou Formation. Samples from the base of the Kayitou Formation and its upper part contain few high-reflectance inertinite macerals but abundant low-reflectance inertinite (Fig. 3). Analysis of the correlation between inertinite content and reflectance revealed an insignificant correlation (Fig. 6a), indicating that wildfire type does not affect inertinite preservation. The data from this study therefore permits reconstruction of the P–T palaeo-wildfire scenario.

5. Discussion

5.1. Wildfire types and the evolution of floral communities

Our research data suggests that the inertinite preserved in the Xuanwei Formation was mainly formed by surface fires with low combustion temperatures (Fig. 3 and Fig. 6b). During deposition of the upper part of the Xuanwei Formation, wildfire types gradually changed to high-temperature crown fires. However, at the base of the Kayitou Formation, inertinite was once again mainly formed by surface fires with low combustion temperatures. Above that level, inertinite formed by high-temperature crown fires dominates the middle part of the Kayitou Formation (Fig. 3 and Fig. 6b), a level that records the second Hg/TOC peak in our study (Fig. 3). In the upper part of the Kayitou Formation, inertinite formed by low-temperature surface fires is dominant again (Fig. 3 and Fig. 6b).

Fire types are closely related to vegetation status. Generally, denser, complex multi-tiered vegetation leads to a variety of wildfire types, while barren conditions experience only a single wildfire type. Due to its palaeogeographic location, southwestern China experienced a humid climate during the late Permian and this region was the last refuge of the Paleozoic pteridophyte–dominated Cathaysian (*Gigantopteris*) Flora (Yu et al., 2015; Xu et al., 2022; Shao et al., 2023). Late Permian peat-forming plant ecosystems, dominated by *Gigantopteris* and *Gigantonoclea* are widely distributed in the South China Plate. These plants, together with *Lobatannularia*, *Paracalamites*, and *Pecopteris* flourished in the warm, humid tropical climate and provided abundant fuel for fires. However, modern broad-leaved, closed forests have a litter that decomposes readily under perpetually warm, dark, moist conditions. They tend to be constantly wet, reducing the presence of flammable surface fuels. This suppresses fire and results in these close forests generally being considered fire-resistant (Belcher et al., 2010; Staver et al., 2011; Nascimento et al., 2022), despite comprising fire-intollerant species (Clarke et al., 2014). Although the high oxygen concentration of the late Permian atmosphere was conducive to combustion and the spread of fire, fires in their initial stages were typically of low intensity and at ground level (He and Lamont, 2018; Yan et al., 2019). These types of fire spread relatively slowly, with fires often girdling tree trunks and occurring in a highly mosaic fashion (Mays and McLoughlin, 2022). In addition, anomalous warming and a short-term reduction in precipitation may have promoted and sustained wetland wildfires in the late Permian. In the case of wetland fires, once rainforests have burned, the community structure is changed, affecting the ambient relative humidity and rendering vegetation more vulnerable to more intense fires (Cochrane, 2003). These studies provide important context for inferred changes in wildfire types seen in our borehole succession, particularly in the upper part of the Xuanwei Formation (stage 1 and stage 2 in Fig. 7). The enhanced wildfires at that level might have impacted the last wetland communities that are represented by the topmost coals in the late Permian (Fig. 3 and stage 2 in Fig. 7), threatening many plant and animal species with extinction.

The first peak in inertinite contents is at the base of the Kayitou Formation, and this peak is associated with low inertinite reflectance, a negative $\delta^{13}C_{org}$ excursion, and a sedimentary Hg peak (Fig. 3). Palaeontological investigation has revealed that the vegetation shifts in southwestern China occurred above the last coal of the Xuanwei Formation (Yu et al., 2015; Xu et al., 2022; Shao et al., 2023). In the lower part of the Kayitou Formation, the residual holdovers of the *Gigantopteris* flora together with "Triassic-type" plant fossils such as *Tomiostrobus* (*Annalepis)*, constituted a distinct *Annalepis–Peltaspermum* assemblage (Yu et al., 2015). The palaeogeographic environment had become a near-barren landscape dominated by herbaceous lycophytes during deposition of the lower part of the Kayitou Formation (Feng et al., 2020; Xu et al., 2022). Prolonged dry seasons may render rainforests vulnerable to fire. Due to the increase in fire frequencies, previously dominant woody species do not have enough time to complete their life cycles, in which case only herbs could survive (Scheiter et al., 2012). In this case, although the abnormally high temperatures driven by contemporaneous STLIP volcanism enhanced the frequency of surface wildfires, these types of wildfires were only surficial and high-temperature crown fires did not occur at that time due to the lack of combustible material (stage 3 in Fig. 7). It has been reported that in the immediate aftermath of the terrestrial PTME plant crisis, plants underwent modest recovery with an increase in abundance and diversity of conifers and ferns (Xu et al., 2022; Shao et al., 2023). Subsequently, plant diversity gradually increased with drought-tolerant conifer-dominated floras replacing fern-dominated communities (Xu et al., 2022; Shao et al., 2023). Our spore/pollen ratio analysis shows that the relative abundance of pollen increased and gradually became dominant in the Kayitou Formation (Fig. 3). Some gymnosperms have a suite of functional traits allowing persistence under wildfire regimes, such as retaining old branches and releasing seeds in response to fire (He and Lamont, 2018). It should be noted that the dominance of pollen is common after frequent surface

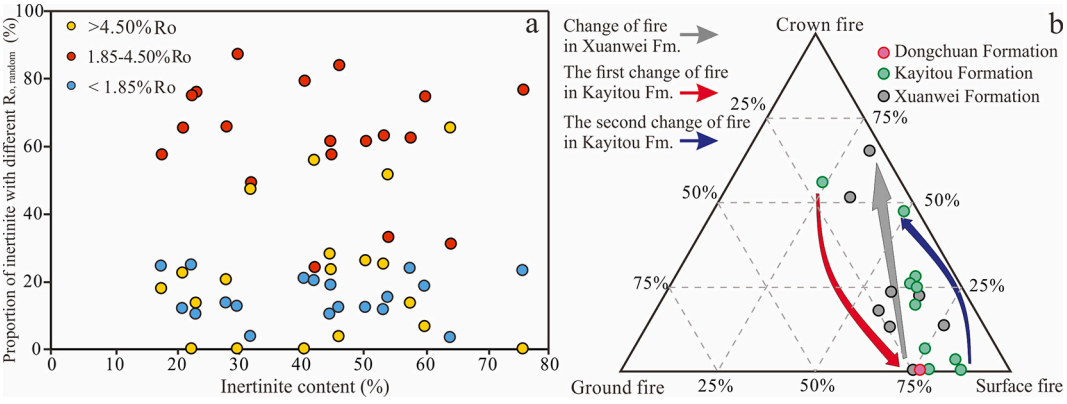

Fig. 6. Scatter plot of reflectance of inertinite vs. content of inertinite and fire type variation. a correlation between the reflectance of inertinite and the content of inertinite; b fire types change in the Xuanwei, Kayitou and Dongchuan formations: the Xuanwei Formation shows an increasing trend, the Kayitou Formation shows decreasing first and then decreasing, and the Dongchuan Formation stays at a low level.

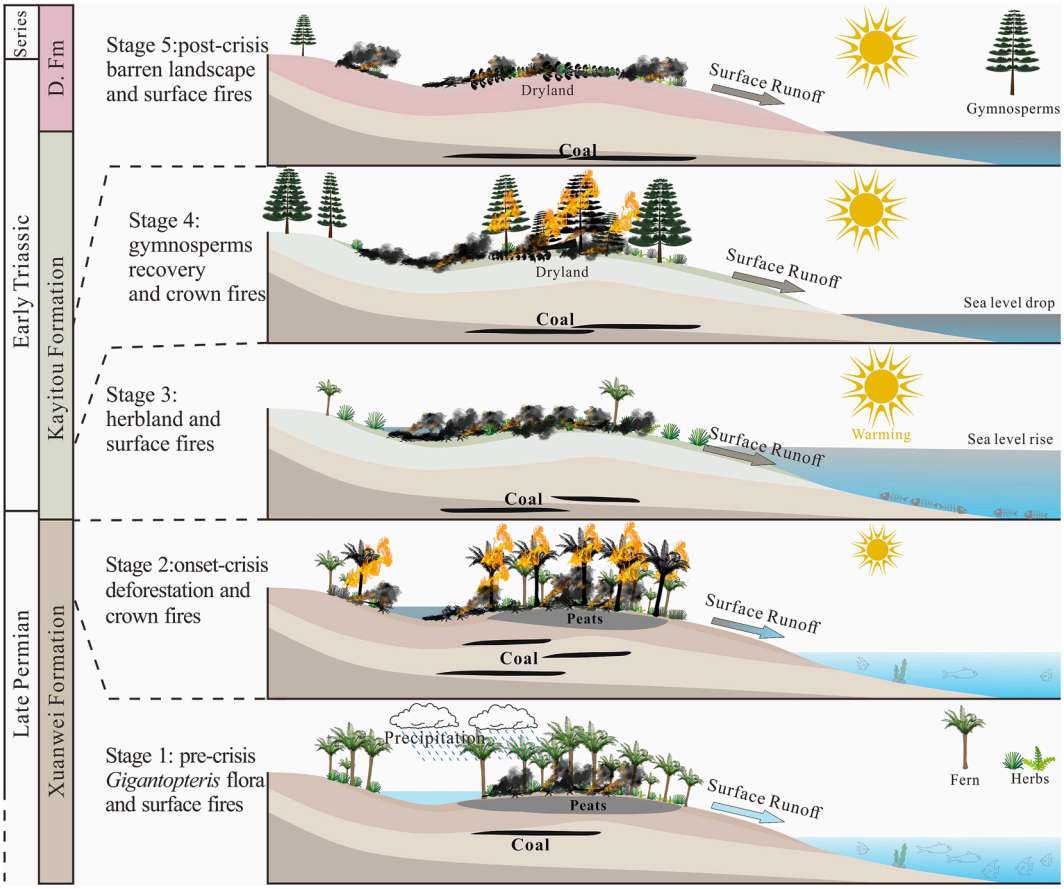

Fig. 7. Schematic model illustrating possible relationships between the wildfires and floral changes during the P–T transition in southwestern China.

fires, probably because fires clear space for opportunistic plant species. In the P–T transition the opportunistic lycopsid *Tomiostrobus* was eventually replaced after the plant crisis as gymnosperms gradually occupied the empty niches during deposition of the lower part of the Kayitou Formation (Feng et al., 2020; Xu et al., 2022; Shao et al., 2023). Probably due to the addition of gymnosperms, fuel for fires again became abundant, and high-temperature crown fire activity resumed by the time that the middle part of the Kayitou Formation was deposited (Fig. 3 and stage 4 in Fig. 7). Although there is no irrefutable evidence that these gymnosperms were tall woody plants (Xu et al., 2022; Shao et al., 2023), the higher values of inertinite reflectance and inferred higher combustion temperatures are consistent with the dominance of crown fires, in turn suggesting that plants at that time were not restricted to low herbaceous types. With global warming and drought further stressing terrestrial ecosystems in the Early Triassic, drought-tolerant conifer-dominated floras flourished, but this created a tipping point in diversity (Xu et al., 2022; Shao et al., 2023), and the final, widespread plant extinctions occurred during deposition of the upper part of the Kayitou Formation. Wildfires are known not only for their destructive power – they are intrinsically linked to renewal and change of vegetation, with associated impacts for terrestrial ecosystems (He and Lamont, 2018).

In the aftermath of the culmination of the terrestrial crisis, the palaeogeographic environment in southwestern China evolved into a near-barren landscape by the time that the Dongchuan Formation was deposited (Zhang et al., 2016; Feng et al., 2020; Shao et al., 2023). At this time, crown fire activity subsided, and surface and ground fires probably eliminated the last plant groups that had clung on during deposition of the uppermost part of the Kayitou Formation (Fig. 3 and stage 5 in Fig. 7).

5.2. *Wildfires and the terrestrial PTME*

Many PTME records from non-marine sections are less well-constrained in terms of the placement of the P–T boundary and the duration of the extinction itself (Wignall et al., 2020). The drivers of the terrestrial crisis are not clear, with some drivers (such as acid rain and ozone disruption) being inferred by indirect, often local evidence (Dal Corso et al., 2022). Since evidence of wildfires has been reported across the PTME interval in terrestrial settings, and also from the marine succession at the GSSP at Meishan (Shen et al., 2011; Kaiho et al., 2020; Cai et al., 2021a), enhanced wildfire activity has been implicated as a key driver of the terrestrial PTME. Wildfires can directly kill forests and they also release gases and particulates into the atmosphere, with potentially damaging effects on terrestrial ecology (Benton, 2018; Kelly et al., 2020). The effects of wildfire on surface vegetation can also lead to increased soil erosion (Fig. 3), causing large amounts of sediment to be transported into the marine system through surface runoff (Yan et al., 2019). In our study, the highest inertinite/charcoal abundances are known from the interval between the latest Permian coal and a level several metres above (Shao et al., 2012; Yan et al., 2019; Vajda et al., 2020; Cai et al., 2021b; Mays and McLoughlin, 2022), representing a duration of wildfire activity longer than that of terrestrial ecosystem collapse. This raises questions about the relationship between wildfires and the terrestrial PTME. Fig. 8 synthesizes and correlates data from numerous sections across the South China Plate, including the Meishan GSSP. We use this correlation to evaluate the relationship between wildfires and changes in terrestrial ecosystems (Fig. 8). The presence of negative $\delta^{13}C$ excursions, Hg/TOC spikes and high-precision zircon U—Pb dates for the PTME interval provides a useful correlative tool between different terrestrial and marine records (Chu et al., 2020; Wignall et al., 2020; Wu et al., 2024). From this correlation, we conclude

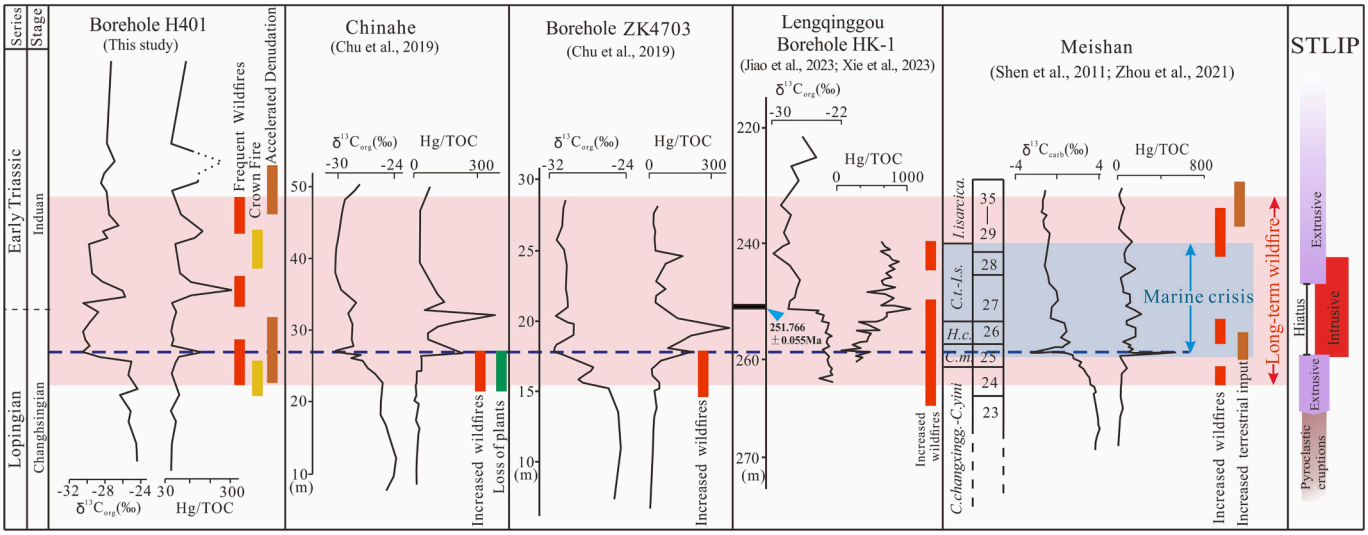

Fig. 8. Compilation of $\delta^{13}C_{org}$, Hg/TOC ratios and wildfire activities through the P–T transition in South China. The data from Chinahe and ZK4703 is from Chu et al., 2020; the data of Lengqinggou is from Cai et al., 2021b. Chen et al., 2023, Jiao et al., 2023, and Wu et al., 2024; $\delta^{13}C_{org}$ and Hg/TOC data from Meishan is from Wang et al., 2021; and wildfires and terrestrial input at Meishan is from Zhou et al., 2021. The magmatic phases of the STLIP are from Burgess et al. (2017). Blue dashed line = correlation of the major negative $\delta^{13}C_{org}$ excursion and the Hg/TOC peak. (For interpretation of the references to colour in this figure legend, the reader is referred to the web version of this article.)

that wildfires were extensive for a long time before and after the main pulse of the marine crisis in the South China Plate (Fig. 8).

Several previous studies have suggested that wildfires played a major role in the dramatic disruption of terrestrial ecology and that wildfires might have caused the collapse of the peatland ecosystem in southern China during the PTME (Shen et al., 2011; Shao et al., 2012; Zhang et al., 2016). We suggest that intense wildfires might not have eradicated plants during sudden, brief intervals during the P–T transition but instead the effects of fire were cumulative in driving forest transformations. In turn, the response of forests probably controlled the types of wildfires that occurred. Today, forest fires are widespread, with much of the Earth's surface subject to periodic fires (Bowman et al., 2009). However, wildfires are not generally thought to cause the complete collapse of forest ecosystems (He and Lamont, 2018).

Increasing evidence suggests that the onset of the terrestrial PTME predates the marine extinction (Fielding et al., 2019; Chu et al., 2020; Guo et al., 2022; Lu et al., 2022). Although it seems unlikely that wildfires alone destroyed terrestrial ecosystems, enhanced wildfires could have made forest systems more vulnerable to other stresses (He and Lamont, 2018). The first phase of the terrestrial extinction coincided with the initial, mostly effusive-pyroclastic phase of the STLIP (Burgess et al., 2017; Chu et al., 2020). Wildfires, along with this initial volcanism (with probable causal relationships), apparently contributed to this earlier disturbance in terrestrial (vs. marine) settings. During the late Permian, wildfires played a role in disrupting the stability of the forest systems. Burning vegetation would have released significant amounts of CO_2 and pollutants such as polycyclic aromatic hydrocarbons (PAHs), influencing the carbon cycle and regional climate (Cai et al., 2021a; Song et al., 2022; Jiao et al., 2023). Furthermore, during the post-fire period, the loss of the vegetation cover and the physical barrier that intercepts rainfall would have enhanced surface runoff and denudation (Vajda et al., 2020; Yang et al., 2022; Hua et al., 2023). It has been postulated that a large amount of terrestrial debris and black carbon were transported into the ocean by rivers, leading to increased turbidity and marine productivity (Yan et al., 2019). However, in southwestern China, late Permian and earliest Triassic strata lack organic–rich mudstone facies such as black shales to evidence this process, leading Wignall et al. (2020) to postulate that the organic matter was trapped in alluvial and fluvial facies by marine transgression. Events on land may have driven ecological stress in the ocean even before terrestrial ecosystems completely collapsed. The subsequent STLIP intrusive phase exerted a fatal blow to the by-now fragile ecosystem, and the concomitant warming of 8–10 °C proved enough to kill most life (Wang et al., 2020a). During this phase, frequent surface fires cleared the last Paleozoic flora, creating room for the new Mesozoic flora. As temperatures and rainfall changed through time, drought-tolerant gymnosperms gradually became the dominant group in the Early Triassic. During this transition, ongoing frequent wildfire and volcanic activity may have delayed the full recovery of terrestrial ecosystems. Eventually, the later phase of Early Triassic deforestation removed the woody gymnosperms in southwestern China, promoting a second acceleration in denudation rates (Zhou et al., 2021; Huang et al., 2022; Yang et al., 2022; Hua et al., 2023). Wildfire activities seem to have persisted as long as there were plants providing combustible material.

5.3. A volcanic driver of climate change and wildfires

Volcanically-driven environmental change is generally considered the driver of the PTME (Wignall, 2001; Sobolev et al., 2011; Lu et al., 2020; Wang et al., 2021; Dal Corso et al., 2022) with the STLIP being seen as the main culprit (Burgess et al., 2017). Numerous studies have shown that volcanism can trigger calamitous global environmental changes (e.g., global warming) through the release of CO_2, SO_2 and other volatiles, plus toxic metals, and many of these have been implicated in the PTME (Cui et al., 2017; Wang et al., 2021; Li et al., 2022). Global warming, anoxia and oceanic acidification are oft-cited drivers of the marine crisis (Dal Corso et al., 2022). The main STLIP intrusive phase and gas emissions began at 251.907 ± 0.067 Ma and are associated with marine losses that occurred in a < 100 kyr interval that straddled the P–T boundary (Burgess et al., 2014; Shen et al., 2019b). Sedimentary mercury (Hg) contents have become a powerful proxy for major volcanism in the geological record (Grasby et al., 2019) and Hg concentration peaks are known from the terrestrial P–T boundary in the South China Plate (Shen et al., 2011; Shen et al., 2019a; Chu et al., 2020). As shown here and elsewhere, the close correspondence of Hg/TOC peaks and stable carbon isotopes fluctuations during the P–T transition suggests that massive quantities of isotopically light CO_2 (~36,000 Gt C) were released by volcanism before entering the ocean and atmosphere (Shen et al., 2011; Zhang et al., 2021; Cui et al., 2021). These abundant greenhouse gases drove extreme warming and sea

surface temperatures reached 40 °C, leading to catastrophic mass extinction (Joachimski et al., 2012; Sun et al., 2012; Benton, 2018; Wang et al., 2020a). The marked increase in the rate of denudation indicates a strong shift in the terrestrial hydrological cycle (Fig. 3). The disruption of the hydrological cycle combined with the extreme high temperatures at the end of the Permian may have promoted aridity on land (Sun et al., 2012; Retallack, 2013; Benton, 2018). Frequent and intense wildfires may be thus a function of global warming (Baker, 2022). As well as the data presented in this study, abundant charcoal from wildfires has been reported from P–T strata elsewhere in the South China Plate (Shen et al., 2011; Chu et al., 2020; Cai et al., 2021b), in the North China Plate (Dal Corso et al., 2022; Lu et al., 2022) and in eastern Australia (Vajda et al., 2020). Given the regional differences in climate and biotas, this prevalence of fire was likely caused by a (volcanically-driven) global shift in climate, including warming and enhanced seasonality (Mays and McLoughlin, 2022).

In this study, the horizons with abundant inertinite or charcoals are also levels of elevated Hg/TOC peaks, suggesting there is potentially a causal link between volcanism and wildfire (Fig. 3). We suggest that climate changes, driven by volcanism, promoted more frequent wildfires during the P–T interval (Baker, 2022). In addition, the most important natural heat source to ignite vegetation is lightning, which has been a feature of Earth throughout its history (He and Lamont, 2018). In the modern day, lightning occurs nearly 1.4 billion times per year globally and its frequency increases with climate warming (Chen et al., 2021). Global warming during the P–T interval likely greatly increased the frequency of lightning at that time, resulting in more frequent fires. Zhang et al. (2021) proposed that large-scale felsic eruptions injected massive quantities of S, Cu and Hg into the South China Block during the P–T transition, which could have been responsible for a regional crisis. The pyroclasts released by regional volcanic eruptions might also have been an important ignition source in forests (Zhang et al., 2021). The widely distributed volcanic ash layer and tonsteins in the late Permian to earliest Triassic strata in South China also support a scenario in which regional volcanism drove elevated regional wildfire activity (He et al., 2014). Hence, volcanism both in the South China Plate, and further afield in the STLIP seems to have driven climate change and wildfires, together causing irreversible damage to terrestrial ecosystems during the P–T transition.

6. Conclusions

1) The high proportion of inertinite in the upper part of the Xuanwei Formation and the lower part of the Kayitou Formation indicates that enhanced wildfires were prevalent during the P–T transition. The abundant inertinite accompanied by a Hg/TOC peak in the earliest Triassic suggests that volcanism and wildfires co-existed, supporting a causal relationship between these phenomena.
2) The multi-tiered *Gigantopteris* forests in lowland peat mires promoted crown fire in the latest Permian, while the barren upland dominated by herbaceous lycophytes saw surface fires in the earliest Triassic. The subsequent invasion of gymnosperms led to the resumption of crown fires. The relationship between wildfires and plants is complex, but it is not one of total destruction - instead, the removal of some material promoted changes in terrestrial environments as seen in the records of shifting vegetation in this study.
3) Wildfires were pervasive over a long time in the P–T interval in southwestern China. Wildfires burned prior to the initial extinction phase and thus fire is unlikely to be the sole cause of the collapse of terrestrial ecosystems. Enhanced wildfire destroyed the stability of wetlands prior to the main extinction phase and frequent wildfire and inhospitable conditions inhibited the recovery of terrestrial ecology in the post-extinction aftermath.

CRediT authorship contribution statement

Fanghui Hua: Writing – review & editing, Writing – original draft, Methodology, Investigation, Formal analysis, Data curation. **Longyi Shao:** Writing – review & editing, Writing – original draft, Supervision, Resources, Project administration, Methodology, Investigation, Funding acquisition, Formal analysis, Data curation, Conceptualization. **Xuetian Wang:** Writing – review & editing, Methodology, Investigation, Formal analysis. **Timothy P. Jones:** Writing – review & editing, Writing – original draft, Supervision, Methodology, Formal analysis, Conceptualization. **Tianchang Zhang:** Writing – review & editing, Methodology, Investigation, Formal analysis. **David P.G. Bond:** Writing – review & editing, Methodology, Funding acquisition, Formal analysis. **Zhiming Yan:** Methodology, Investigation, Formal analysis. **Jason Hilton:** Writing – review & editing, Supervision, Methodology, Funding acquisition, Conceptualization.

Declaration of competing interest

The authors declare that they have no known competing financial interests or personal relationships that could have appeared to influence the work reported in this paper.

Data availability

All data used in the paper is included in the paper or as part of the supplementary files

Acknowledgements

This study is supported by the Science Fund for Creative Research Groups of the National Natural Science Foundation of China (Grant No. 42321002), the National Natural Science Foundation of China (Grant No. 41572090, 42102213, and 42302126), and the Natural Environmental Research Council (UK, Award NE/P013724/1).

Appendix A. Supplementary data

Supplementary data to this article can be found online at https://doi.org/10.1016/j.palaeo.2024.112129.

References

Alexander, M.E., Stocks, B.J., Wotton, B.M., Flannigan, M.D., Todd, J.B., Butler, B.W., Lanoville, R.A., 1998. The international crown fire modelling experiment: an overview and progress report. In: Second Symposium on Fire and Forest Meteorology, 11–16 January 1988. American Meteorological Society, Boston, USA, pp. 20–23.

Ali, J.R., Thompson, G.M., Zhou, M.F., Song, X., 2005. Emeishan large igneous province, SW China. Lithos 79, 475–489. https://doi.org/10.1016/j.lithos.2004.09.013.

Baker, S.J., 2022. Fossil evidence that increased wildfire activity occurs in tandem with periods of global warming in Earth's past. Earth Sci. Rev. 224, 103871 https://doi.org/10.1016/j.earscirev.2021.103871.

Batten, D.J., 1996. Palynofacies and palaeoenvironmental interpretation. In: Jansonius, J., McGregor, D.C. (Eds.), Palynology: Principles and Applications, 3. American Association of Stratigraphic Palynologists Foundation, Los Angeles, pp. 1011–1064 (Chapter26A).

Belcher, C.M., Hudspith, V.A., 2016. The formation of charcoal reflectance and its potential use in post-fire assessments. Int. J. Wildland Fire 25, 775–779. https://doi.org/10.1071/WF15185.

Belcher, C.M., Mander, L., Rein, G., Jervis, F.X., Haworth, M., Hesselbo, S.P., Glasspool, I. J., McElwain, J.C., 2010. Increased fire activity at the Triassic/ Jurassic boundary in Greenland due to climate-driven floral change. Nat. Geosci. 3, 426–429.

Benton, M.J., 2018. Hyperthermal-driven mass extinctions: killing models during the Permian-Triassic mass extinction. Philos. Trans. R. Soc. A 376, 2130. https://doi.org/10.1098/rsta.2017.0076.

Benton, M.J., Newell, A.J., 2014. Impacts of global warming on Permo-Triassic terrestrial ecosystems. Gondwana Res. 25 (4), 1308–1337. https://doi.org/10.1016/j.gr.2012.12.010.

Bercovici, A., Cui, Y., Forel, M.B., Yu, J.X., Vajda, V., 2015. Terrestrial paleoenvironment characterization across the Permian–Triassic boundary in South China. J. Asian Earth Sci. 98, 225–246. https://doi.org/10.1016/j.jseaes.2014.11.016.

Bowman, D.M., Balch, J.K., Artaxo, P., Bond, W.J., Carlson, J.M., Cochrane, M.A., D'Antonio, C.M., Defries, R.S., Doyle, J.C., Harrison, S.P., Johnston, F.H., Keeley, J. E., Krawchuk, M.A., Kull, C.A., Marston, J.B., Moritz, M.A., Prentice, I.C., Roos, C.I., Scott, A.C., Swetnam, T.W., van der Werf, G.R., Pyne, S.J., 2009. Fire in the Earth system. Science 324 (5926), 481–484. https://doi.org/10.1126/science.116388.

Broutin, J., Yu, J.X., Shi, X., Shu, W.C., Qing, X., 2020. Terrestrial palaeofloral succession across the Permian–Triassic boundary in the North and South China blocks: a brief review. PalZ 94 (4), 633–644. https://doi.org/10.1007/s12542-020-00511-0.

Burgess, S.D., Bowring, S., Shen, S.Z., 2014. High-precision timeline for Earth's most severe extinction. Proc. Natl. Acad. Sci. USA 111 (9), 3316–3321. https://doi.org/10.1073/pnas.1317692111.

Burgess, S.D., Muirhead, J.D., Bowring, S.A., 2017. Initial pulse of Siberian Traps sills as the trigger of the end-Permian mass extinction. Nat. Commun. 8 (1), 164. https://doi.org/10.1038/s41467-017-00083-9.

Cai, Y.F., Zhang, H., Cao, C.Q., Zheng, Q.F., Jin, C.F., Shen, S.Z., 2021a. Wildfires and deforestation during the Permian–Triassic transition in the southern Junggar Basin, Northwest China. Earth-Sci. Rev. 218, 103670 https://doi.org/10.1016/j.earscirev.2021.103670.

Cai, Y.F., Zhang, H., Feng, Z., Shen, S.Z., 2021b. Intensive wildfire associated with volcanism promoted the vegetation changeover in Southwest China during the Permian−Triassic transition. Front. Earth Sci. 9, 615841 https://doi.org/10.3389/fe2021.615841.

Chen, Z.Q., Benton, M.J., 2012. The timing and pattern of biotic recovery following the end-Permian mass extinction. Nat. Geosci. 5, 375–383. https://doi.org/10.1038/ngeo1475.

Chen, Y., Romps, D.M., Seeley, J.T., Veraverbeke, S., Riley, W.J., Mekonnen, Z.A., Randerson, J.T., 2021. Future increases in Arctic lightning and fire risk for permafrost carbon. Nat. Clim. Chang. 11 (5), 404–410. https://doi.org/10.1038/s41558-021-01011-y.

Chen, J.B., Sun, G.Y., Lu, B.J., Ma, R.Y., Xiao, Z., Cai, Y.F., Zhang, H., Shen, S.Z., Zhang, F.F., Feng, Z., 2023. Inconsistent mercury records from terrestrial upland to coastal lowland across the Permian-Triassic transition. Earth Planet. Sci. Lett. 614, 118195.

Chu, D.L., Yu, J.X., Tong, J.N., Benton, M.J., Song, H.J., Huang, Y.F., Song, T., Tian, L., 2016. Biostratigraphic correlation and mass extinction during the Permian-Triassic transition in terrestrial-marine siliciclastic settings of South China. Glob. Planet. Chang. 146, 67–88. https://doi.org/10.1016/j.gloplacha.2016.09.009.

Chu, D.L., Grasby, S.E., Song, H.J., Corso, J.D., Wang, Y., Mather, T.A., Wu, Y.Y., Song, H.Y., Shu, W.C., Tong, J.N., Wignall, P.B., 2020. Ecological disturbance in tropical peatlands prior to marine Permian-Triassic mass extinction. Geology 48 (3), 288–292. https://doi.org/10.1130/G46631.1.

Clarke, P.J., Prior, L.D., French, B.J., Vincent, B., Knox, K.J.E., Bowman, D.M.J.S., 2014. Using a rainforest-flame forest mosaic to test the hypothesis that leaf and litter fuel flammability is under natural selection. Oecologia 176, 1123–1133.

Cochrane, M.A., 2003. Fire science for rainforests. Nature 421, 913–919.

Cui, Y., Bercovici, A., Yu, J.X., Kump, L.R., Freeman, K.H., Su, S., Vajda, V., 2017. Carbon cycle perturbation expressed in terrestrial Permian–Triassic boundary sections in South China. Glob. Planet. Chang. 148, 272–285. https://doi.org/10.1016/j.gloplacha.2015.10.018.

Cui, Y., Li, M.S., van Soelen, E.E., Peterse, F., Kürschner, W.M., 2021. Massive and rapid predominantly volcanic CO_2 emission during the end-Permian mass ex-tinction. Proc. Natl. Acad. Sci. USA 118, 2014701118. https://doi.org/10.1073/pnas.2014701118.

Dal Corso, J., Song, H., Callegaro, S., Chu, D., Sun, Y., Hilton, J., Grasby, S.E., Joachimski, M.M., Wignall, P.B., 2022. Environmental crises at the Permian–Triassic mass extinction. Nat. Rev. Earth Environ. 3, 197–214. https://doi.org/10.1038/s43017-021-00259-4.

Feng, Z., Wei, H.B., Guo, Y., He, X.Y., Sui, Q., Zhou, Y., Liu, H.Y., Gou, X.D., Lv, Y., 2020. From rainforest to herbland: new insights into land plant responses to the end-Permian mass extinction. Earth Sci. Rev. 204, 103153 https://doi.org/10.1016/j.earscirev.2020.103153.

Fielding, C.R., Frank, T.D., McLoughlin, S., Vajda, V., Mays, C., Tevyaw, A.P., Winguth, A., Winguth, C., Nicoll, R.S., Bocking, M., Crowley, J.L., 2019. Age and pattern of the southern high-latitude continental end-Permian extinction constrained by multiproxy analysis. Nat. Commun. 10, 385. https://doi.org/10.1038/s41467-018-07934-z.

Glasspool, I.J., Scott, A.C., 2010. Phanerozoic concentrations of atmospheric oxygen reconstructed from sedimentary charcoal. Nature Geoscience 3 (9), 627–630.

Glasspool, I.J., Scott, A.C., Waltham, D., Pronina, N., Shao, L.Y., 2015. The impact of fire on the late Paleozoic Earth system. Front. Plant Sci. 6, 756.

Grasby, S.E., Them, T.R., Chen, Z.H., Yin, R.S., Ardakani, O.H., 2019. Mercury as a proxy for volcanic emissions in the geologic record. Earth Sci. Rev. 196, 102880 https://doi.org/10.1016/j.earscirev.2019.102880.

Guo, W.W., Tong, J.N., He, Q., Hounslow, M.W., Song, H.J., Dal Corso, J., Wignall, P.B., Ramezani, J., Tian, L., Chu, D.L., 2022. Late Permian–Middle Triassic magnetostratigraphy in North China and its implications for terrestrial-marine correlations. Earth Planet. Sci. Lett. 585, 117519 https://doi.org/10.1016/j.epsl.2022.117519.

He, T., Lamont, B.B., 2018. Baptism by fire: the pivotal role of ancient conflagrations in evolution of the Earth's flora. Natl. Sci. Rev. 5 (2), 237–254. https://doi.org/10.1093/nsr/nwx041.

He, B., Zhong, Y.T., Xu, Y.G., Li, X.H., 2014. Triggers of Permo-Triassic boundary mass extinction in South China: the Siberian Traps or Paleo-Tethys ignimbrite flare-up? Lithos 204, 258–267. https://doi.org/10.1016/j.lithos.2014.05.011.

Hua, F.H., Shao, L.Y., Zhang, T.C., Bond, D.P.G., Wang, X.T., Wang, J., Yan, Z.M., Lu, J., Hilton, J., 2023. An astronomical timescale for the Permian-Triassic mass extinction reveals a two-step, million-year-long terrestrial crisis in South China. Earth Planet. Sci. Lett. 605, 118035 https://doi.org/10.1016/j.epsl.2023.118035.

Huang, B.C., Yan, Y.G., Piper, J.D.A., Zhang, D.H., Yi, Z.Y., Yu, S., Zhou, T.H., 2018. Paleomagnetic constraints on the paleogeography of the East Asian blocks during late Paleozoic and early Mesozoic times. Earth Sci. Rev. 186, 8–36. https://doi.org/10.1016/j.earscirev.2018.02.004.

Huang, Y.F., He, W.H., Liao, W., Wang, Y.B., Yi, Z.X., Yang, H., Li, G.S., 2022. Two pulses of increasing terrestrial input to marine environment during the Permian–Triassic transition. Palaeogeogr. Palaeoclimatol. Palaeoecol. 586, 110753 https://doi.org/10.1016/j.palaeo.2021.110753.

International Committee for Coal and Organic Petrology (ICCP), 2001. The new inertinite classification (ICCP System, 1994). Fuel 80, 459–471. https://doi.org/10.1016/S0016-2361(00)00102-2.

Jiao, S.L., Zhang, H., Cai, Y.F., Chen, J.B., Feng, Z., Shen, S.Z., 2023. Collapse of tropical rainforest ecosystems caused by high-temperature wildfires during the end-Permian mass extinction. Earth Planet. Sci. Lett. 614 (2023), 118193 https://doi.org/10.1016/j.epsl.2023.118193.

Joachimski, M.M., Lai, X.L., Shen, S.Z., Jiang, H.S., Luo, G.M., Chen, B., Chen, J., Sun, Y. D., 2012. Climate warming in the latest Permian and the Permian-Triassic mass extinction. Geology 40 (3), 195–198. https://doi.org/10.1130/G32707.1.

Jolly, W.M., Cochrane, M.A., Freeborn, P.H., Holden, Z.A., Brown, T.J., Williamson, G.J., Bowman, D.M., 2015. Climate-induced variations in global wildfire danger from 1979 to 2013. Nat. Commun. 6, 7537.

Jones, T.P., 1997. Fusain in Late Jurassic Sediments from Witch Ground Graben, North Sea, U.K, 58. Mededelingen Nederlands Instituut voor. Toegepaste Geowetenschappen TNO, pp. 93–103.

Jones, T.P., Chaloner, W.G., 1991. Fossil charcoal, its recognition and paleoatmospheric significance. Palaeogeogr. Palaeoclimatol. Palaeoecol. 97, 39–50. https://doi.org/10.1016/0031-0182(91)90180-Y.

Jones, T.P., Scott, A.C., Cope, M., 1991. Reflectance measurements and the temperature of formation of modern charcoals and implications for studies of fusain. Bull. Soc. Geol. Fr. 162, 193–200.

Kaiho, K., Aftabuzzaman, M., Jones, D.S., Tian, L., 2020. Pulsed volcanic combustion events coincident with the end-Permian terrestrial disturbance and the following global crisis. Geology 49, 289–293.

Kamo, S.L., Czamanske, G.K., Amelin, Y., Fedorenko, V.A., Davis, D.W., Trofimov, V.R., 2003. Rapid eruption of Siberian flood-volcanic rocks and evidence for coincidence with the Permian-Triassic boundary and mass extinction at 251 Ma. Earth Planet. Sci. Lett. 214, 75–91. https://doi.org/10.1016/S0012-821X(03)00347-9.

Kelly, L.T., Giljohann, K.M., Duane, A., Aquilue, N., Archibald, S., Batllori, E., Bennett, A. F., Buckland, S.T., Canelles, Q., Clarke, M.F., Fortin, M.J., Hermoso, V., Herrando, S., Keane, R.E., Lake, F.K., McCarthy, M.A., Moran-Ordonez, A., Parr, C.L., Pausas, J.G., Penman, T.D., Regos, A., Rumpff, L., Santos, J.L., Smith, A.L., Syphard, A.D., Tingley, M.W., Brotons, L., 2020. Fire and biodiversity in the anthropocene. Science 370, 6519. https://doi.org/10.1126/science.abb0355.

Krause, A.J., Mills, B.J.W., Zhang, S., Planavsky, N.J., Lenton, T.M., Poulton, S.W., 2018. Stepwise oxygenation of the Paleozoic atmosphere. Nat. Commun. 9, 4081. https://doi.org/10.1038/s41467-018-06383-y.

Li, M.H., Frank, T.D., Xu, Y.L., Fielding, C.R., Gong, Y.Z., Shen, Y.A., 2022. Sulfur isotopes link atmospheric sulfate aerosols from the Siberian Traps outgassing to the end-Permian extinction on land. Earth Planet. Sci. Lett. 592, 117634 https://doi.org/10.1016/j.epsl.2022.117634.

Lindström, S., 2021. Two-phased mass rarity and extinction in land plants during the end-Triassic climate crisis. Front. Earth Sci. 9, 780343 https://doi.org/10.3389/feart.2021.780343.

Lu, J., Zhang, P.X., Yang, M.F., Shao, L.Y., Hilton, J., 2020. Continental records of organic carbon isotopic composition ($\delta^{13}C_{org}$), weathering, paleoclimate and wildfire linked to the end-Permian mass extinction. Chem. Geol. 558, 119764 https://doi.org/10.1016/j.chemgeo.2020.119764.

Lu, J., Wang, Y., Yang, M.F., Zhang, P.X., Bond, D.P.G., Shao, L.Y., Hilton, J., 2022. Diachronous end-Permian terrestrial ecosystem collapse with its origin in wildfires. Palaeogeogr. Palaeoclimatol. Palaeoecol. 594, 110960 https://doi.org/10.1016/j.palaeo.2022.110960.

Mays, C., McLoughlin, S., 2022. End-Permian burnout: the role of Permian–Triassic wildfires in extinction, carbon cycling, and environmental change in eastern Gondwana. Palaios 37 (6), 292–317. https://doi.org/10.2110/palo.2021.051.

Nascimento, M.N., Heijink, B.M., Bush, M.B., Gosling, W.D., McMichael, C.N.H., 2022. Early to mid-Holocene human activity exerted gradual influences on Amazonian forest vegetation. Philos. Trans. R. Soc. Lond. Ser. B Biol. Sci. 377, 1849. https://doi.org/10.1098/rstb.2020.0498.

Peng, Y.Q., Yu, J.X., Gao, Y.Q., Yang, F.Q., 2006. Palynological assemblages of non-marine rocks at the Permian–Triassic boundary, western Guizhou and eastern Yunnan, South China. J. Asian Earth Sci. 28 (4–6), 291–305. https://doi.org/10.1016/j.jseaes.2005.10.007.

Retallack, G.J., 2013. Permian and Triassic greenhouse crises. Gondwana Res. 24 (1), 90–103. https://doi.org/10.1016/j.gr.2012.03.003.

Riel, N., Jaillard, E., Martelat, J.-E., Guillot, S., Braun, J., 2018. Permian-Triassic Tethyan realm reorganization: implications for the outward Pangea margin. J. S. Am. Earth Sci. 81, 78–86. https://doi.org/10.1016/j.jsames.2017.11.007.

Scheiter, S., Higgins, S.I., Osborne, C.P., Bradshaw, C., Lunt, D., Ripley, B.S., Taylor, L.L., Beerling, D.J., 2012. Fire and fire-adapted vegetation promoted C4 expansion in the late Miocene. New Phytol. 195, 653–666.

Scott, A.C., 1989. Observations on the nature and origin of fusain. Int. J. Coal Geol. 12, 443–475. https://doi.org/10.1016/0166-5162(89)90061-X.

Scott, A.C., 2010. Charcoal recognition, taphonomy and uses in palaeoenvironmental analysis. Palaeogeogr. Palaeoclimatol. Palaeoecol. 291, 11–39. https://doi.org/10.1016/j.palaeo.2009.12.012.

Scott, A.C., Glasspool, I.J., 2005. Charcoal reflectance as a proxy for the emplacement temperature of pyroclastic flow deposits. Mater. Sci. Forum 33, 865–868. https://doi.org/10.1130/G21474.1.

Scott, A.C., Glasspool, I.J., 2007. Observations and experiments on the origin and formation of inertinite group macerals. Int. J. Coal Geol. 70, 53–66. https://doi.org/10.1016/j.coal.2006.02.009.

Shao, L.Y., Wang, H., Yu, X.H., Lu, J., Zhang, M.Q., 2012. Paleo-fires and atmospheric oxygen levels in the latest Permian: evidence from maceral compositions of coals in eastern Yunnan, southern China. Acta Geol. Sin.-Engl. 86 (4), 949–962. https://doi.org/10.1111/j.1755-6724.2012.00719.x.

Shao, L.Y., Gao, C.X., Zhang, C., Wang, H., Guo, L.J., Gao, C.H., 2013. Sequence-Palaeogeography and coal accumulation of late Permian in Southwestern China. Acta Sedi. Sci. 31 (5), 856–866 (in Chinese with English abstract).

Shao, L.Y., Wang, X.T., Wang, D.D., Li, M.P., Wang, S., Li, Y.J., Shao, K., Zhang, C., Gao, C.X., Dong, D.X., Cheng, A.G., Lu, J., Ji, C.W., Gao, D., 2020. Sequence stratigraphy, paleogeography, and coal accumulation regularity of major coal-accumulating periods in China. Int. J. Coal Sci. Technol. 7 (2), 240–262. https://doi.org/10.1007/s40789-020-00341-0.

Shao, L.Y., Hua, F.H., Wang, J., Ji, X.K., Yan, Z.M., Zhang, T.C., Wang, X.T., Ma, S.M., Jones, T.P., Lu, H.N., 2023. Palynological dynamics in the late Permian and the Permian–Triassic transition in southwestern China. Palaeogeogr. Palaeoclimatol. Palaeoecol. 619, 111540 https://doi.org/10.1016/j.palaeo.2023.111540.

Shen, S.Z., Crowley, J.L., Wang, Y., Bowring, S.A., Erwin, D.H., Sadler, P.M., Cao, C.Q., Rothman, D.H., Henderson, C.M., Ramezani, J., Zhang, H., Shen, Y., Wang, X.D., Wang, W., Mu, L., Li, W.Z., Tang, Y.G., Liu, X.L., Liu, L.J., Zeng, Y., Jiang, Y.F., Jin, Y.G., 2011. Calibrating the end-Permian mass extinction. Science 334, 1367–1372. https://doi.org/10.1126/science.1213454.

Shen, J., Yu, J.X., Chen, J.B., Algeo, T.J., Xu, G.Z., Feng, Q.L., Shi, X., Planavsky, N.J., Shu, W.C., Xie, S.C., 2019a. Mercury evidence of intense volcanic effects on land during the Permian-Triassic transition. Geology 47 (12), 1117–1121. https://doi.org/10.1130/G46679.1.

Shen, S.Z., Ramezani, J., Chen, J., Cao, C.Q., Erwine, D.H., Zhang, H., Xiang, L., Erwin, D.H., Henderson, C.M., Zhen, F.Q., Bowring, S.A., Wang, Y., Li, X.H., Wang, X.D., Yuan, D.X., Zhang, Y.C., Mu, L., Wu, Y.S., 2019b. A sudden end-Permian mass extinction in South China. Geol. Soc. Am. Bull. 131, 205–223. https://doi.org/10.1130/B31909.1.

Sobolev, S.V., Sobolev, A.V., Kuzmin, D.V., Krivolutskaya, N.A., Petrunin, A.G., Arndt, N. T., Radko, V.A., Vasiliev, Y.R., 2011. Linking mantle plumes, large igneous provinces and environmental catastrophes. Nature 477, 312–316. https://doi.org/10.1038/nature10385.

Song, H.J., Wignall, P.B., Tong, J.N., Yin, H.F., 2013. Two pulses of extinction during the Permian-Triassic crisis. Nat. Geosci. 6, 52–56. https://doi.org/10.1038/ngeo1649.

Song, Y., Tian, Y., Yu, J.X., Algeo, T.J., Luo, G.M., Chu, D.L., Xie, S.C., 2022. Wildfire response to rapid climate change during the Permian-Triassic biotic crisis. Glob. Planet. Chang. 215, 103872 https://doi.org/10.1016/j.gloplacha.2022.103872.

Stanley, S.M., 2016. Estimates of the magnitudes of major marine mass extinctions in earth history. Proc. Natl. Acad. Sci. USA 113 (42), E6325–E6334. https://doi.org/10.1073/pnas.1613094113.

Staver, A.C., Archibald, S., Levin, S.A., 2011. The global extent and determinants of savanna and forest as alternative stable states. Science 334, 230–232.

Sun, Y.D., Joachimski, M.M., Wignall, P.B., Yan, C.B., Chen, Y.L., Jiang, H.S., Wang, L.N., Lai, X.L., 2012. Lethally hot temperatures during the Early Triassic greenhouse. Science 338 (6105), 366–370. https://doi.org/10.1126/science.1224126.

Vajda, V., Raine, J.I., Hollis, C.J., 2001. Indication of global deforestation at the Cretaceous-Tertiary boundary by New Zealand fern spike. Science 294, 1700–1702. https://doi.org/10.1126/science.1064706.

Vajda, V., McLoughlin, S., Mays, C., Frank, T.D., Fielding, C.R., Tevyaw, A., Lehsten, V., Bocking, M., Nicoll, R.S., 2020. End-Permian (252 Mya) deforestation, wildfires and flooding—an ancient biotic crisis with lessons for the present. Earth Planet. Sci. Lett. 529, 115875 https://doi.org/10.1016/j.epsl.2019.115875.

Wang, J., Shao, L.Y., Wang, H., Spiro, B., Large, D., 2018. SHRIMP zircon U-Pb ages from coal beds across the Permian–Triassic boundary, eastern Yunnan, southwestern China. J. Palaeogeogr. 7 (2), 117–129. https://doi.org/10.1016/j.jop.2018.01.002.

Wang, W.Q., Garbelli, C., Zhang, F.F., Zheng, Q.F., Zhang, Y.C., Yuan, D.X., Shi, Y.K., Chen, B., Shen, S.Z., 2020a. A high-resolution middle to late Permian paleotemperature curve reconstructed using oxygen isotopes of well-preserved brachiopod shells. Earth Planet. Sci. Lett. 540, 116245 https://doi.org/10.1016/j.epsl.2020.116245.

Wang, X.T., Shao, L.Y., Eriksson, K.A., Yan, Z.M., Wang, J.M., Li, H., Zhou, R.X., Lu, J., 2020b. Evolution of a plume-influenced source-to-sink system: an example from the coupled Central Emeishan large igneous province and adjacent western Yangtze cratonic basin in the late Permian, SW China. Earth-Sci. Rev. 207, 103224 https://doi.org/10.1016/j.earscirev.2020.103224.

Wang, X.D., Cawood, P.A., Grasby, S.E., Zhao, L.S., Chen, Z.Q., Wu, S.L., Huang, Y.G., 2021. Characteristics of Hg concentrations and isotopes in terrestrial and marine facies across the end-Permian mass extinction. Glob. Planet. Chang. 205, 103592 https://doi.org/10.1016/j.gloplacha.2021.103592.

Wignall, P.B., 2001. Large igneous provinces and mass extinctions. Earth Sci. Rev. 53 (1–2), 1–33. https://doi.org/10.1016/S0012-8252(00)00037-4.

Wignall, P.B., Chu, D.L., Hilton, J.M., Dal Corso, J., Wu, Y.X., Wang, Y.C., Atkinson, J., Tong, J.N., 2020. Death in the shallows: the record of Permo-Triassic mass extinction in paralic settings, Southwest China. Glob. Planet. Chang. 189, 103176 https://doi.org/10.1016/j.gloplacha.2020.103176.

Wu, Q., 2020. High-Precision Zircon U-Pb Geochronological Studies of the Permian Ash Beds from China and North America, PhD. University of Science and Technology of China (in Chinese with English abstract).

Wu, Q., Zhang, H., Ramezani, J., Zhang, F.F., Erwin, D.H., Feng, Z., Shao, L.Y., Cai, Y.F., Zhang, S.H., Xu, Y.G., Shen, S.Z., 2024. The terrestrial end-Permian mass extinction in the paleotropics postdates the marine extinction. Sci. Adv. 10 (5), eadi7284 https://doi.org/10.1126/sciadv.adi7284.

Xu, Z., Hilton, J., Yu, J.X., Wignall, P.B., Yin, H.F., Xue, Q., Ran, W.J., Hui, L., Shen, J., Meng, F.S., 2022. End-Permian to Middle Triassic plant species richness and abundance patterns in South China: coevolution of plants and the environment through the Permian-Triassic transition. Earth Sci. Rev. 232, 104136 https://doi.org/10.1016/j.earscirev.2022.104136.

Yan, Z.M., Shao, L.Y., Glasspool, I.J., Wang, J., Wang, X.T., Wang, H., 2019. Frequent and intense fires in the final coals of the Paleozoic indicate elevated atmospheric oxygen levels at the onset of the end-Permian mass extinction event. Int. J. Coal Geol. 207, 75–83. https://doi.org/10.1016/j.coal.2019.03.016.

Yang, J.H., Cawood, P.A., Condon, D.J., Liu, J.Z., Deng, X.S., Wang, J.F., Du, Y.S., Yuan, D.X., 2022. Anomalous weathering trends indicate accelerated erosion of tropical basaltic landscapes during the Permo-Triassic warming. Earth Planet. Sci. Lett. 577, 117256 https://doi.org/10.1016/j.epsl.2021.117256.

Yin, H.F., Tong, J.N., Ding, M.H., Zhang, K.X., Lai, X.D., 1994. Late Permian-Middle Triassic sea level changes of Yangtze platform. Earth Sci. 19, 627–632 (in Chinese with English abstract).

Yu, J.X., Broutin, J., Chen, Z.Q., Shi, X., Li, H., Chu, D.L., Huang, Q.S., 2015. Vegetation changeover across the Permian–Triassic boundary in southwest China: extinction, survival, recovery and palaeoclimate: a critical review. Earth Sci. Rev. 149, 203–224. https://doi.org/10.1016/j.earscirev.2015.04.005.

Zhang, G.W., Guo, A.L., Wang, Y.J., Li, S.Z., Dong, Y.P., Liu, S.F., He, D.F., Cheng, S.Y., Lu, R.K., Yao, A.P., 2013. Tectonics of South China continent and its implications. Sci. China Earth Sci. 56, 1804–1828. https://doi.org/10.1007/s11430-013-4679-1 (in Chinese with English abstract).

Zhang, H., Cao, C.Q., Liu, X.L., Mu, L., Zheng, Q.F., Liu, F., Xiang, L., Liu, L.J., Shen, S.Z., 2016. The terrestrial end-Permian mass extinction in South China. Palaeogeogr. Palaeoclimatol. Palaeoecol. 448, 108–124. https://doi.org/10.1016/j.palaeo.2015.07.002.

Zhang, H., Zhang, F.F., Chen, J.B., Erwin, D.H., Syverson, D.D., Ni, P., Rampino, M., Chi, Z., Cai, Y.F., Xiang, L., Li, W.Q., Liu, S.G., Wang, R.C., Wang, X.D., Feng, Z., Li, H.M., Zhang, T., Cai, H.M., Zheng, W., Cui, Y., Zhu, X.K., Hou, Z.Q., Wu, F.Y., Xu, Y.G., Planavsky, N., Shen, S.Z., 2021. Felsic volcanism as a factor driving the end-Permian mass extinction. Sci. Adv. 7, eabh1390 https://doi.org/10.1126/sciadv.abf8142.

Zhou, W., Algeo, T.J., Luo, G., Ruan, X., Chen, Z.Q., Xie, S.C., 2021. Hydrocarbon compound evidence in marine successions of South China for frequent wildfires during the Permian-Triassic transition. Glob. Planet. Chang. 200, 103472 https://doi.org/10.1016/j.gloplacha.2021.103472.